42nd AIAA Aerospace Sciences Meeting and Exhibit
5 - 8 January 2004, Reno, Nevada

AIAA 2004-979

Structure of Locally Quenched Swirl Stabilized Turbulent Premixed Flames

G. Eggenspieler* and S. Menon†
School of Aerospace Engineering
Georgia Institute of Technology
Atlanta, Georgia 30332
gte075x@prism.gatech.edu, suresh.menon@ae.gatech.edu

Large Eddy Simulations (LES) of turbulent premixed combustion close to Lean Blow Out (LBO) in a gas turbine engine have been performed. A sub-grid combustion model based on the linear-eddy mixing (LEM) model is implemented to simulate premixed combustion over a wide range of operational conditions, including combustion near LBO. Pollutant (CO and NO) formation is predicted using transport models and by using different chemical mechanisms. For simple chemical mechanism, it is possible to predict emission of pollutants using a flamelet approach and with a flame extinction model. However, when no extinction model is employed but a more detailed chemical mechanism (which exhibits extinction in the laminar limit) is used no extinction is observed even though decrease in both OH and fuel reaction rate is observed in regions of high stretch. Analysis suggests that flame stretching and its effect on flame propagation are captured, but not all the relevant scales involved in flame extinction are properly resolved. In particular, it is shown that eddies smaller than 4-5$\overline{\Delta}$ but larger than $\overline{\Delta}$ (LES grid resolution) are important scales that impact local flame quenching. However, with the current resolution, such eddies are not resolved properly and therefore, quenching is not predicted. A possible approach to deal with this problem without a drastic increase in LES resolution (and the associated cost) is suggested.

1 Introduction

State-of-the-art gas turbines engines using Lean-Premix-Prevaporized (LPP) technology operate at equivalence ratio slightly higher than the lean extinction limit value. Turbulent combustion process taking place under these conditions does not necessarily satisfy the condition for combustion in the flamelet regime, where the flame thickness (δ_F) is smaller than the Kolmogorov scale (η) and the chemical time scales (τ_C) is smaller than the characteristic turbulent flow time scales (τ_F). Other turbulent combustion regimes may also be locally present and the combustion may occur in the Thin-Reaction Zone (TRZ) regime (where the flame front can be broadened by eddies having length scales smaller or comparable to the flame front thickness) and/or in the Broken Reaction- Zone (BRZ) regime where the concept of a connected flame surface is highly questionable (see Fig. 1). Therefore, a modeling approach must be able to deal with all these regimes without requiring ad hoc changes.

Experimental studies under laboratory conditions[1, 2] have shown that, in highly turbulent flows, the flame preheat zone is only moderately modified and the reaction zone is unperturbed. This is confirmed by numerical and experimental studies of laminar flame / vortex interactions.[3, 4] Therefore, flamelet models are often used in studies of combustion process in a gas turbine combustion chamber. Under this assumption, the flame structure is assumed to be laminar-like, i.e., turbulent structures do not affect the flame reaction zone and only moderately affect the preheat zone. These conditions are likely to occur in gas turbine engines as long as the operating condition is far from the lean flammability limit.

On the other hand, near the lean limit, flame extinction can occur since the turbulent Reynolds number is very high in the mixing region under typical gas turbine operation, and the flame structure may not be able to sustain itself in this region. Physically, such flame quenching is expected in the BRZ regime, where eddies can penetrate and alter the reaction zone. Another source of flame quenching is stretch generated by eddies larger than the flame thickness.[5] Both these phenomena cannot be predicted by classical flamelet models and new approaches are needed to account for flame quenching near LBO. Recent studies have identified that flame extinction is also of particular importance when CO emission prediction is considered.[6, 7]

From a modeling perspective, in order to predict or simulate flame extinction, all chemical and turbulent length and time scales have to be resolved or their effects have to be modeled accurately. Direct numerical simulation (DNS) with detailed kinetics could address this problem accurately but the computational cost is

*Graduate Research Assistant
†Professor, AIAA Associate Fellow

beyond current or even future processing capability. LES may offer a viable alternative but, even in LES, some simplifications are necessary in order to make the problem computationally tractable. In the LES approach, scales larger than the grid size $\overline{\Delta}$ are expected to be resolved while scales smaller that $\overline{\Delta}$ have to be modeled. If the grid is coarse (and this is necessary for LES to be computationally efficient), the effect of missing scales have to be properly accounted in the sub-grid model. A related issue is that, in practice, to resolve a typical eddy on the LES grid around 4-5 grid points are needed. This suggests that scales below $4\text{-}5\overline{\Delta}$ are not resolved in a LES and have to be modeled in some manner.

Modeling the sub-grid scales (i.e. scales below $\overline{\Delta}$) using, for example, an eddy viscosity approach[8] may be acceptable for the momentum transport closure but is problematic for scalar transport since species mix at the molecular level and therefore, mixing at the small-scale is very important. Experiments have demonstrated that even in isotropic turbulence, scalar fields can be highly anisotropic.[9] This suggests that the micro-scale scalar structure is very important for proper prediction of the mixed fluid, and hence for predicting combustion. Thus, in the lean limit, the effect of missing scales needs to be included accurately in order to predict flame structure and the associated dynamics.

In this study, we visit this rather complex problem using an approach that attempts to address these issues. A sub-grid *simulation* method based on the Linear-Eddy Mixing (LEM)[10] model is employed to treat chemical reaction, sub-grid molecular diffusion and small-scale turbulent stirring within the sub-grid as an alternate to modeling their effects on the LES grid. The ability of this approach within LES (called LEMLES, hereafter) is addressed using a realistic problem of lean combustion in a premixed dump combustor used in power generation gas turbines.

A General Electric LM 6000 gas turbine combustor with nominal operating conditions and inflow conditions is used for these studies.

Earlier,[11,12,13,14] combustion in the flamelet-TRZ regimes were studied extensively and the results were compared to experimental data. Very good agreement was demonstrated by both a thin-flame model[11,12] and by LEMLES for conditions far from LBO.[14] We revisit this device for the same flow conditions but now using a much leaner mixture.

2 Model Formulation

2.1 LES Formulation

The governing equations of motion for an unsteady, compressible, reacting, multi-species fluid are the Navier-Stokes equations describing the conservation of mass, momentum, total energy and N-species. In the LES methodology, the large scale motion is fully resolved on the computational grid using a time- and space-accurate scheme and only the small scales are modeled. The separation between the large (resolved) and the small (unresolved) scales is determined by the grid size ($\overline{\Delta}$). A Favre spatial top-hat filter (which is appropriate for the finite-volume scheme employed here) is employed to derive the LES equations.[15] The filtered Navier Stokes equations for mass, momentum, energy conservation and their closure will only be described briefly here but information can be found elsewhere.[11]

A Favre spatial top-hat filter (which is appropriate for the finite-volume scheme employed here) is employed to derive the LES equations.[15] Thus, any variable (f) is decomposed into a resolved quantity ($\widetilde{f}$) and a unresolved (quantity (f'') such that $f = \widetilde{f} + f''$. The resulting LES equations are:[11]

$$\begin{cases} \frac{\partial \overline{\rho}}{\partial t} + \frac{\partial \overline{\rho}\widetilde{u_i}}{\partial x_i} = 0 \\ \frac{\partial \overline{\rho}\widetilde{u_i}}{\partial t} + \frac{\partial}{\partial x_j}\Big[\overline{\rho}\widetilde{u_i}\widetilde{u_j} + \overline{p}\delta_{ij} - \overline{\tau_{ij}} + \tau_{ij}^{sgs}\Big] = 0 \\ \frac{\partial \overline{\rho}\widetilde{E}}{\partial t} + \frac{\partial}{\partial x_i}\Big[\Big(\overline{\rho}\widetilde{E} + \overline{p}\Big)\widetilde{u}_i + \\ \overline{q_i} - \widetilde{u}_j\overline{\tau_{ji}} + H_i^{sgs} + \sigma_i^{sgs}\Big] = 0 \end{cases}$$

In the above equations, u_i is the i-th velocity component, ρ is the mass density, p is the pressure and $E = e + \frac{1}{2}(u_k^2 + k^{sgs})$ is the total energy. Here, e is the internal energy per unit mass computed as the sum of the sensible enthalpy and the chemical stored energy, and k^{sgs} is the sub-grid kinetic energy (defined below). Also, q_i is the heat flux vector and τ_{ij} is the viscous stress tensor, given by $\tau_{ij} = \mu\Big(\partial u_i/\partial x_j + \partial u_j/\partial x_i\Big) - \frac{2}{3}\mu\Big(\partial u_k/\partial x_k\Big)\delta_{ij}$. Here, μ is the molecular viscosity coefficient which is determined using the Sutherland's law.

In the LES equations, all the above variables appear in their filtered form and many of these terms require closure. Some simplifications are required as well. For example, the filtered viscous shear stress ($\overline{\tau_{ij}}$) and heat flux ($\overline{q_i}$) are approximated using the filtered velocity. The non-linear terms in the equations, upon filtering result in unclosed terms that represent the effect of the unresolved motion on the resolved field. These are: τ_{ij}^{sgs}, H_i^{sgs} and σ_i^{sgs} and are respectively, the sub-grid shear stress, the sub-grid heat flux and the the sub-grid viscous stress. These terms are defined as follows:

$$\begin{cases} \tau_{ij}^{sgs} = \overline{\rho}\Big[\widetilde{u_iu_j} - \widetilde{u}_i\widetilde{u}_j\Big] \\ H_i^{sgs} = \overline{\rho}\Big[\widetilde{Eu_i} - \widetilde{E}\widetilde{u}_i\Big] + \Big[\overline{pu_i} - \overline{p}\widetilde{u}_i\Big] \\ \sigma_i^{sgs} = \overline{u_j\tau_{ji}} - \widetilde{u}_j\overline{\tau_{ji}} \end{cases} \quad (1)$$

2.2 Subgrid Closure

The closure of sub-grid terms is a major area of research and many approaches have been proposed in the past. In general, since the small-scales primarily provide dissipation for the energy that cascades from the large scales through the inertial range, an eddy viscosity type sub-grid model appears appropriate to model the sub-grid stresses τ_{ij}^{sgs} and heat flux H_i^{sgs}. Assuming that an eddy viscosity ν_T can be prescribed, these sub-grid fluxes can be approximated as:

$$\begin{cases} \tau_{ij}^{sgs} = -\nu_T \left(\frac{\partial \widetilde{u_i}}{\partial x_j} + \frac{\partial \widetilde{u_j}}{\partial x_i} \right) \\ H_i^{sgs} = -\nu_T \frac{\partial \widetilde{h}}{\partial x_i} \end{cases} \tag{2}$$

To obtain the sub-grid eddy viscosity ν_T, a characteristic length scale L^{sgs} and a characteristic velocity scale V^{sgs} for the unresolved scales of motion must be identified and prescribed, since the simplest model for ν_T is $\nu_T = C_\nu L^{sgs} V^{sgs}$. Here, C_ν is a coefficient of proportionality. In LES, the grid resolution $\overline{\Delta}$ is typically chosen as the characteristic length scale of the smallest resolved (or alternatively, the largest unresolved) eddy. However, as noted earlier, numerically the smallest eddy that can be resolved requires at least 3-4 grid points which implies that this choice is not necessarily correct but is within the range of acceptable length scales.

Subgrid models for eddy viscosity differ primarily in the prescription of the velocity scale, V^{sgs}. Earlier LES studies[16] used the resolved strain rate $S_{ij} = \frac{1}{2}(\frac{\partial \widetilde{u_i}}{\partial x_j} + \frac{\partial \widetilde{u_j}}{\partial x_i})$ and $\overline{\Delta}$ to obtain V^{sgs} such that $V^{sgs} = \overline{\Delta} S$ where $S = (S_{ij} S_{ij})^{1/2}$. With this closure, an algebraic eddy viscosity model is obtained and such a model has been employed in many simulations in the past. However, a limitation of this model is that the formal derivation of this eddy viscosity expression requires that production and dissipation of the turbulent kinetic energy must be in equilibrium. Since this requirement is only satisfied in the dissipation scales, proper application of the algebraic model requires that the entire inertial range is resolved. This requirement is very severe for high Re flows since the overall grid resolution required to meet this criteria can exceed available resource by a substantial amount. Therefore, for complex, high-Re flows, an alternate choice of the velocity scale is needed.

Here, we employ a transport model for the sub-grid kinetic energy k^{sgs} to obtain V^{sgs}. This model is described below.

2.3 Subgrid Turbulent Kinetic Energy

A transport equation is formally derived for k^{sgs} and solved along with the rest of the LES equations. Since k^{sgs} evolves locally and temporally in the flow, the equilibrium assumption is relaxed and now, the cutoff between the resolved and the unresolved scales can be in the inertial range instead of the dissipation range. Thus, a relatively coarse grid can be used to simulate LES of high Re flows. Past studies[17,18,11,12] have demonstrated the ability and accuracy of this model.

The k^{sgs} transport model is given as:

$$\frac{\partial \overline{\rho} k^{sgs}}{\partial t} + \frac{\partial}{\partial x_i}\left(\overline{\rho} \widetilde{u_i} k^{sgs} \right) = P^{sgs} - D^{sgs} + \frac{\partial}{\partial x_i}\left(\frac{\overline{\rho} \nu_T}{Pr_T} \frac{\partial k^{sgs}}{\partial x_i} \right) \tag{3}$$

Here, the subgird kinetic energy is defined as $k^{sgs} = \frac{1}{2}\left[\widetilde{u_k^2} - \widetilde{u_k}^2 \right]$, and Pr_T is a sub-grid Prandtl number, assumed to be unity.

In the above equation, P^{sgs} and D^{sgs} represent respectively, the production and dissipation of the subgrid kinetic energy. These terms are modeled as follow:

$$P^{sgs} = -\tau_{ij}^{sgs} \frac{\partial \widetilde{u_i}}{\partial x_j} \tag{4}$$

$$D^{sgs} = C_\epsilon \overline{\rho} (k^{sgs})^{3/2} / \overline{\Delta} \tag{5}$$

The sub-grid stress using k^{sgs} model is then obtained as:

$$\tau_{ij}^{sgs} = -2\overline{\rho}\nu_T \left(\widetilde{S_{ij}} - \frac{1}{3}\widetilde{S_{kk}}\delta_{ij} \right) + \frac{2}{3}\overline{\rho} k^{sgs} \delta_{ij} \tag{6}$$

where the sub-grid eddy viscosity is given by

$$\nu_T = C_\nu (k^{sgs})^{1/2} \overline{\Delta} \tag{7}$$

In the above equation, two model coefficients C_ϵ and C_ν appear and they must be prescribed or obtained dynamically as a part of the solution. Earlier studies[18,11,12] established a localized dynamic approach that did not employ the Germono's identity rather employed a scale-similarity closure. This approach resulted in a robust and stable approach for determining the model coefficients locally in the combustor without requiring any averaging or smoothing. In the present study, we employ constant values of $C_\nu = 0.067$ and $C_\epsilon = 0.916$ that were established earlier using theoretical and numerical studies of high-Re stagnation point premixed flames.[19,20] Localized dynamic evaluation of the model coefficients will be considered in the near future but the results reported here are not expected to be very sensitive to this issue.

2.4 LEMLES Formulation

In conventional LES, the scalar conservation equations are solved using an Eulerian technique and subgrid closure models are needed to close the sub-grid scalar flux and the reaction rate terms. Closure of both these terms can be problematic when multi-species (with widely different molecular diffusivity) finite-rate

kinetics have to be studied. In LEMLES, scalars conservation equations are solved on a one-dimensional computational domain, also called LEM domain, embedded in every LES cells. Although details of this procedure have been given elsewhere,[21,14] we summarize some of the salient features of this method. Consider the transport equation for a scalar ψ and split the velocity field according to the LES technique: $u = \widetilde{u} + u'$.

$$\frac{\partial \psi}{\partial t} = -\widetilde{u_k}\frac{\partial \psi}{\partial x_k} - u'_k\frac{\partial \psi}{\partial x_k} + \frac{\partial}{\partial x_m}\left[D_\psi \frac{\partial \psi}{\partial x_m}\right] + w_\psi \quad (8)$$

where D_ψ is the molecular diffusion coefficient and w_ψ is the chemical reaction source term. In LEMLES, the two-scale numerical procedure is represented as:

$$\frac{\psi^* - \psi^n}{\Delta t_{LES}} = -\widetilde{u_k}\frac{\partial \psi}{\partial x_k} - \left(u'_k\right)^{face}\frac{\partial \psi}{\partial x_k} \quad (9)$$

$$\psi^{n+1} - \psi^n = \int_t^{t+\Delta t_{LES}} \left[u'_k\frac{\partial \psi}{\partial x_k} + \frac{\partial}{\partial x_m}\left(D_\psi \frac{\partial \psi}{\partial x_m}\right) + w_\psi\right] dt \quad (10)$$

Equation 9 describes the large-scale 3D LES-resolved convection of the scalar field and is implemented via the transfer of fluid volumes between LES control volumes through the control volume surfaces. The convection by the term $\left(u'_k\right)^{face}$ is the convection of the scalars through the control volume surfaces due to the sub-grid velocity field. Equation 10 describes the sub-grid stirring via $\int_t^{t+\Delta t_{LES}} u'_k \frac{\partial \psi}{\partial x_k} dt$, the sub-grid molecular diffusion and reaction kinetics that occur within each LES cell.

Since the sub-grid resolution is assumed sufficient to resolve all scales below the LES grid scale, reaction and diffusion processes are included in an exact manner within the 1D domain. This exact closure is similar to the closure in PDF methods[22] except that, unlike in PDF methods, molecular diffusion (and hence, differential diffusion) effects can also be included in the LEMLES. As in PDF methods, the large-scale transport (Eq. 9) is modeled as a Lagrangian transport of the scalar fields across LES cells and the sub-grid turbulent stirring is modeled. In PDF methods, the Curl's coalescence-dispersion mixing model is often employed to model turbulent mixing, whereas in LEMLES, small-scale turbulent stirring is implemented using a scalar rearrangement process that mimics the action of an eddy upon the scalar field.[10] The location of this stirring event is chosen from a uniform distribution and the frequency of stirring is derived from 3D inertial range scaling laws derived from Kolmogorov's hypothesis as:

$$\lambda = \frac{54}{5}\frac{\nu Re_{\overline{\Delta}}}{C_\lambda \overline{\Delta}^3}\frac{[(\overline{\Delta}/\eta)^{5/3} - 1]}{[1 - (\eta/\overline{\Delta})^{4/3}]} \quad (11)$$

C_λ represent the scalar turbulent diffusivity and is determined as 0.067. The eddy size (l) is chosen from the following PDF:

$$f(l) = \frac{(5/3)l^{-8/3}}{\eta^{-5/3} - \overline{\Delta}^{-5/3}} \quad (12)$$

where $\eta = N_\eta \overline{\Delta} Re_{\overline{\Delta}}^{-4/3}$. The empirical constant N_η reduces the effective range of scales between the integral length scale and η but does not change the turbulent diffusivity ($N_\eta \in [1.3;10.78]$).

It has been demonstrated that the turbulent scaling laws predict correctly the growth of the flame surface area under the influence of turbulent strain. Note that, this model does not require any change when the flame type (premixed or diffusion flame) or the combustion regime (flamelet, TRZ or BRZ regimes) changes. This ability has been demonstrated in the past[23,7] and it is this ability that we believe is crucial to deal with complex phenomenon such as LBO. Further details are given in cited references and therefore, avoided here for brevity.

Conservation of mass, momentum and energy (at the LES level) and conservation of mass, energy and species (at the LEM level) are strongly coupled.[14] Chemical reaction at the LEM level determines heat release and thermal expansion at the LEM level, which at the LES level generates flow motion that, in turns, transports the species field at the LEM level. Full coupling is maintained in the LEMLES to ensure local mass conservation.

2.5 Combustion and Pollutant Modeling

For all the LEMLES studies, finite-rate kinetics is employed within the sub-grid. However, due to computational cost of such simulations, some simplifications have been employed. Three chemical mechanisms are used in this study: a 5-species/1-step global mechanism, a 8-species/4-steps reduced mechanism and a 9-species/5-steps reduced mechanism. These mechanisms are summarized below.

Mechanism A: 5-species/1-step:[24]

$$CH_4 + 2(O_2 + 3.76N_2) \rightleftharpoons CO_2 + 2H_2O + 7.52N_2 \quad (13)$$

Mechanism B: 8-species/4-steps:[25]

$$\begin{aligned} CH_4 + 2H + H_2O &\rightleftharpoons CO + 4H_2 \\ CO + H_2O &\rightleftharpoons CO_2 + H_2 \\ 2H + M &\rightleftharpoons H_2 + M \\ O_2 + 3H_2 &\rightleftharpoons 2H + 2H_20 \end{aligned} \quad (14)$$

Mechanism C: 9-species/5-steps:[26]

$$\begin{aligned} 3H_2 + O_2 + CO_2 &\rightleftharpoons 3H_2 + CO \\ H_2 + 2OH &\rightleftharpoons 2H_2O \\ 3H_2 + CO &\rightleftharpoons H_2O + CH_4 \end{aligned}$$

$$H_2 + CO_2 \rightleftharpoons \quad H_2O + CO$$
$$3H_2 + CO_2 + 2NO \rightleftharpoons \quad 3H_2O + CO + N2 \quad (15)$$

Laminar flame governed by the one-step (Mechanism A) can quench if the Lewis number is larger than unity.[4] Card and *al.*[25] simulated the extinction of a non-premixed methane-air diffusion flame using the Mechanism B (which includes CO). Mechanism C is similar to mechanism B, but also includes both CO and NO.

Both Mechanisms B and C are detailed enough to include CO and UHC emission within the mechanism, but a model is needed to include pollutants when using Mechanism A. In this approach, a model is used to track pollutants (CO, NO and UHC) at the LES level.

A conventional scalar transport model is solved on the LES grid for the pollutants when Mechanism A is employed. However, note that Mechanism A is employed in the LEMLES to predict the global heat release and the flame structure. The LES-resolved transport model for CO, NO and UHC is

$$\frac{\partial \overline{\rho}\widetilde{Y_m}}{\partial t} + \frac{\partial}{\partial x_j}\left[\overline{\rho}\widetilde{Y_m}\widetilde{u_j} - \overline{\rho}D_m\frac{\partial \widetilde{Y_m}}{\partial x_j} + \phi^{sgs}_{j,m} + \Theta^{sgs}_{j,m}\right] = \overline{\rho}\widetilde{\dot{w}_m} \quad (16)$$

$\phi^{sgs}_{j,m}$ is the turbulent sub-grid mass flux and $\Theta^{sgs}_{j,m}$ represents the sub-grid molecular diffusion. Again, in the LEM methodology, $\phi^{sgs}_{j,m}$ is modeled via the triplet mapping method and $\Theta^{sgs}_{j,m}$ is taken into account via diffusion on the LEM domain. However, pollutants are only resolved at the LES level, therefore, $\phi^{sgs}_{j,m}$ is modeled by the classical gradient diffusion model ($\phi^{sgs}_{j,m} = -D_T\frac{\partial \widetilde{Y_m}}{\partial x_i}$) and sub-grid diffusion is neglected. The terms on the right-hand-side of the above equation require closure. If a flamelet structure is assumed, CO and NO at the flame front can be obtained using CHEMKIN-PREMIX[27] by assuming that the local structure is 1D and laminar. In the TRZ and the BRZ regimes, the structure of the flame can differ considerably from a laminar flame, and flame curvature and stretch can also modify emission. Nevertheless, this effect on pollutant formation at the flame front is ignored at present. The laminar flamelet solution can be stored in a library for a range of inflow mixture fractions. The LES-resolved value of a given chemical parameter $\widetilde{\psi}$ depends upon the resolved scale mixture fraction $\widetilde{Z}$, as well as on the level of "unmixedness" of the premixed mixture in a given LES cell, and is measured using the variance of the mixture fraction $\widetilde{Z''}$. In this study, where the mixture is assumed to be perfectly premixed, $\widetilde{Z}$ is constant and $\widetilde{Z''}$ is null.

The closure employed for the filtered reaction rate for the pollutants are summarized in Table 1. The rationale behind these closures is discussed briefly in the following sections.

species	$\widetilde{\dot{w}_m}$
CO	$-\frac{\widetilde{\dot{w}_{CH_4}}}{\widetilde{Z}}Y_{CO,ff} - \frac{1}{\tau_{CO,ox}}\widetilde{Y_{CO,ff}}$ $+\frac{MW_{CO}}{MW_{CH_4}}[UHC][O_2]Aexp\left(\frac{T_A}{T}\right)$
NO	$-\frac{\widetilde{\dot{w}_{CH_4}}}{\widetilde{Z}}Y_{NO,ff} + \frac{1}{\tau_{NO,post-flame}}$
UHC	$-\frac{\widetilde{\dot{w}_{CH_4}}}{\widetilde{Z}}PQF - [UHC][O_2]Aexp\left(\frac{T_A}{T}\right)$

Table 1 Reaction rate closure of the species equations (Eq. 16). All pollutants are tracked at the LES level. PQF is the Portion of Quenched Flame.

2.5.1 Carbon Monoxide

CO is formed and/or destroyed by four major mechanisms: (i) the formation of CO at the flame front, (ii) the oxidation of CO in the post-flame region, (iii) the dissociation of $CO2$ and (iv) the formation of CO via oxidation of unburned $CH4$ (also called UHC). All these mechanisms are modeled explicitly and are summarized in Table 1. A large amount of CO will be produced at the flame front ($Y_{CO,ff}$), and this is obtained using the flamelet library and treated as a jump relationship, i.e., CO production rate at the flame front is proportional to the rate of fuel consumption $\widetilde{\dot{w}_{CH_4}}$.[6,28]

Once CO is formed it will be oxidized into $CO2$. From the flamelet library, the rate of oxidation is given by $\widetilde{\dot{w}}_{CO,ox} = -\frac{1}{\tau_{CO,ox}}\widetilde{Y_{CO}}$. The oxidation time scale is based upon the product temperature at a given equivalence ratio. To account for change in temperature due to heat loss, the CO oxidation time scale is corrected as follow:

$$\frac{1}{\tau_{CO,ox}} = \frac{1}{\tau_{CO,ox}}exp\left(E_A\frac{T - T_B}{T * T_B}\right) \quad (17)$$

Here, $\widetilde{T}$ is the actual LES temperature, T_b is the burnt product temperature (i.e., the adiabatic flame temperature) predicted by the flamelet library, and E_A is the activation energy chosen by curve fitting the flamelet library data. Note that, the reaction rate of CO oxidation in the post-flame region is independent of the sub-grid turbulence since CHEMKIN does not take into account the influence of turbulence.

CO reaches its equilibrium value when the consumption rate equals the production rate via CO_2 dissociation. The flamelet library can be used to determine the CO mass fraction at equilibrium ($Y_{CO,eq}$). The rate of formation of CO via CO_2 dissociation is taken as $\widetilde{\dot{w}_{CO,eq}} = P_b\left(\frac{1}{\tau_{CO,eq}}\right)Y_{CO,eq}$ where P_b=0 on the reactant side and P_b=1 on the product side. When $\widetilde{Y_{CO}} = Y_{CO,eq}$, then $\widetilde{\dot{w}_{CO,eq}} + \widetilde{\dot{w}_{CO,ox}} = 0$. The last mechanism of CO formation via oxidation of unburned hydrocarbon (UHC) is treated explicitly, as described below.

2.5.2 Unburnt Hydrocarbons

Intense turbulence combined with heat loss can quench a premixed flame.[29] If the flame front is partially quenched, pockets of unburnt methane (UHC) will be released into the post-flame region and will oxidize at a rate governed by an Arrhenius-law. Prediction of local flame quenching is highly complicated and the only elegant approach is to include heat loss and detailed kinetics. However, this is computationally very expensive and is not addressed when Mechanism A is employed. Although Mechanisms B and C are used the chemical kinetics is relatively detailed heat loss issues are still not addressed.

In Mechanism A, a global one-step model is used to evaluate the impact of UHC on CO emission. The UHC oxidation into CO is computed as:

$$\frac{d[UHC]}{dt} = [UHC]^a[O_2]^b A exp\Big(-\frac{E_A}{RT}\Big) \qquad (18)$$

Mode l	A	a	b	E_A
A[30]	$6.25 * 10^{16}$	-1/3	4/3	23000
B[6]	$6.25 * 10^{16}$	1	1	23000
C[24]	$2.40 * 10^{16}$	1	1	26100

Table 2 Models used for UHC oxidation[31] with the constants used in Eq. 18. In this study, the model C is used.

Earlier[31] three different rate-constant models[24,30] were considered to determine the of CO formation to the UHC oxidation model, and these models are summarized in Table 2. It was determined that only model C showed a good agreement with data in another combustor (DOE-HAT). In the present study, the model C is used as well.

In order to predict the appropriate amount of UHC released into the post-flame zone, it is necessary to model local flame quenching. Currently, no robust model exists to include this effect in an unsteady simulation model (see additional comments about this later). However, a model developed for steady-state application, called the Intermittent Turbulence Net Flame Stretch Model (ITNFS[5]) has some of the necessary features and therefore, is employed in this study. Note that, since the ITNFS model accounts only for extinction via aerodynamic stretch in the steady limit, it is not expected to be valid near LBO where significant unsteady and finite rate effects occur.

2.5.3 Oxides of Nitrogen

Two sources of NO_x formation are taken into account when the transport model is used with Mechanism A. The first source is the production of NO at the flame front (prompt NO) and the second one is the production of nitric monoxide in the post-flame region (thermal NO). These mechanisms are described in details elsewhere.[32] Prompt NO is formed at the flame front and the amount formed ($Y_{NO,ff}$) is given by the library. The rate of formation of NO at the flame front is computed in the same manner as for CO. The rate of formation of NO in the post-flame region is computed using CHEMKIN output and is a constant independent of $\widetilde{Y_{NO}}$.

It should be noted that the above models for CO, UHC and NO are somewhat inconsistent with the notion that scalar mixing and combustion occurs in the sub-grid. However, these models are computationally efficient and are needed when a global mechanism such as the Mechanism A is employed within the LEMLES. When a more detailed mechanism such as Mechanism B or C is used in LEMLES there is no need for these models and the responsibility for predicting pollutant emission depends considerably on the interaction between finite-rate kinetics and turbulence in the LEMLES approach. The ability of the latter approach is addressed in this paper.

3 Numerical Implementation

3.1 Geometry and Operating Conditions

The geometry of the combustion chamber is similar to the GE LM 6000 and is shown on Fig. 2. The length of the combustion chamber is 0.017 m, its radius is 0.045 cm. In this combustor, the premixed mixture enters the cylindrical main chamber in a swirling manner through a cylindrical inflow pipe. The amount of swirl is evaluated by the swirl number S:

$$S = \frac{\int_0^R \rho u w r^2 dr}{R\int_0^R \rho u^2 r dr} \qquad (19)$$

All conditions employed here are similar to the earlier studies[11,12,14] except that in this study, the equivalence ratio Φ of the incoming mixture is changed from the original value of 0.56. The incoming swirl number is 0.67, the inflow pressure is 6.4 atm, and the inflow temperature is 644 K. The Reynolds number, based on the the mean inflow velocity and the inlet radius is 320,000. The incoming premixed mixture equivalence ratio is varied from 0.53 or 0.44 depending upon the simulated case. A random turbulent field of 7 percent is added to the inflow mean velocity and sub-grid intensity also of around 7 percent is used to specify the incoming sub-grid kinetic energy. No-slip adiabatic wall and characteristic based inflow and outflow conditions[33] are employed for all the reported simulations.

3.2 Code Setup and Grid Topology

The compressible LES equations for mass, momentum and energy are solved using a finite-volume scheme that is fourth order in space and second order in time. A parallel MPI code is employed for all simulations. The LEM implementation in the LES is uniquely suited for parallel processing and results in only a 10 percent increase in overall cost even when 8

species are simulated. Inclusion of finite-rate kinetics within the LEM is computationally expensive if direct integration using a stiff solver is employed.[31] However, the CPU cost can be reduced significantly if In-Situ Adaptive Tabulation (ISAT) procedure[34] is employed. In the current study, ISAT is used within each LES cell to evolve the finite-rate kinetics within the LEM.

The typical grid employed for this study is 120x75x80 for the LES domain and 12 cells are used in the LEM within each LES cell. This LEM resolution is considered nominal. The LES grid is clustered in the shear layer to resolve the turbulent structures in this region. To resolve the shear layer and the flame features without any centerline restriction associated with the use of a cylindrical computational mesh, a hybrid grid is used where the centerline region is resolved using a cartesian grid (120x21x21) and the rest of the domain is resolved using a cylindrical grid mesh.

4 Results and Discussion

Various simulations are performed here, and are summarized in Table 3.

case	Φ	Mechanism	Swirl Number
1	0.44	A	0.67
2	0.53	A	0.67
3	0.44	B	0.67
4	0.53	B	0.67
5	0.44	C	0.67
6	0.53	C	0.67

Table 3 Equivalence ratio, Φ, chemical mechanism and swirl number for the different cases

In the following, we focus primarily on the ability of the LEMLES to predict pollutant emission using the various mechanism. Earlier studies[7] have discussed in some details the emission of CO and NO when Mechanism A is employed with the pollutant model described in Section 2.6 above. It was shown in that study that local quenching and formation of UHC was critical for predicting the increase in CO as the equivalence ratio is decreased (a trend that has been observed in experimental studies[35,6]). In the next section, we discuss some of the results obtained using Mechanism A for the current combustor.

When Mechanism B or C is employed in the LEMLES we do not use any model for UHC formation via quenching since these chemical mechanisms have shown (at least in the laminar limit) to exhibit extinction. Thus, if the sub-grid stirring model in the LEMLES is sufficient to provide the unsteady effect of local straining of the flame region then local quenching should be achieved in LEMLES without requiring any explicit models. The present study is focused primarily to investigate this issue.

4.1 Flow Features

Cases 3 and 4 are used to illustrate some other flow features. The flow enters the combustion chamber in a swirling manner and the swirl number (S=0.67) belongs to the regime where the onset of an Internal Recirculation Zone (IRZ) occurs. According to Lilley,[36] vortex breakdown occurs for S>0.6 for reacting flows. The IRZ manifests itself by a decay of the centerline axial velocity. The flow being reversed in the IRZ zone, negative centerline velocity is expected. This is clearly shown on Fig. 3a. For cases 3 and 4, the mean axial velocity decreases and the minima of this decrease is negative. Figure 3b shows the mean axial velocity profiles at various axial location for cases 3 and 4. Region of negative velocity in the vicinity of the centerline indicates the presence of an IRZ. The IRZ for Φ=0.53 is larger than for Φ=0.44. Furthermore, a region of negative axial velocity is present for Φ=0.44, x/R_i>4 and 0.2<r/R<0.75 (R_i being the inflow pipe radius and R the combustion chamber radius). This is directly due to the fact that, at some instant and for the leaner case, the flame is long enough such that fuel is present at the wall of the combustion chamber. This strongly perturb the flow pattern. This phenomena is not observed for the richer mixture case and may explain the difference in velocity profiles for the 2 cases.

Another recirculation region is created by the sudden expansion of the inflow pipe inside the combustion chamber. This outer recirculation zone (ORZ) is clearly shown on 3b. Its length is approximately 1.5 times the length of the step formed by the sudden expansion mentioned above. The length of the ORZ depends only slightly on the equivalence ratio.

4.2 Pollutants Emission using Mechanism A

The pollutant emission predictions (CO, NO and UHC) are reported for cases 1 and 2 (with Mechanism A) in Table 4.

Case	CO	NO	UHC
1	237	1.2	203
2	86	6.62	133

Table 4 CO, NO and UHC emission predictions for different Φ using the Mechanism A and the pollutant transport models. Results are given in ppm.

It can be seen that, as Φ is decreased, CO emission increases rapidly while NO decreases. These trends are consistent with past observations in various premixed combustors.[35,6] The NO emission decreases with decrease in Φ. Lefebvre[37] demonstrated that, for Φ<0.5, the amount of NO formed in the post-flame region is negligible because of the relatively low post-flame temperature. Therefore, for Φ=0.53 (case 2), NO is produced at the flame front and in the post-flame, while NO is only formed in small quantities at

the flame for Φ=0.44 (case 1).

The UHC emission depends on Φ. As the incoming equivalence ratio is decreased, the flame thickness is increased and its burning velocity decreases. Therefore, the flame becomes more sensitive to the large and small scales motion of the flow. Large scale motion is responsible for flame stretching while small scale structures can more easily penetrate the flame preheat zone as the flame thickness increases.[38] Note that, the flow structures are independent of the incoming mixture fraction and are only dependent upon the inflow velocity profile and combustion chamber geometry. In the leaner case (case 1), the flame is more sensitive to the flow features and, as a result, a larger amount of flame quenching (and UHC release) is expected.

The CO emission trend directly follows UHC emission. The assumed incomplete combustion of unburnt CH_4 in the post-flame region leads to the formation of CO. This phenomena has been observed in past studies[6,7] where UHC has been proved to be a key element for accurate prediction of CO emission.

4.3 Flame Structure

Four types of flame structures have been observed in studies of highly turbulent lean premixed flames.[2] In the "flamelet type burning mode" regime, the flame has a laminar structure. Large turbulent scales wrinkle the flame front but have no influence upon the flame structure. In the "thickened preheat zone" regime, the flame is stretch by large-scale structure and smaller eddies can penetrate the preheat zone, thus enhancing turbulent mixing inside the preheat zone. In the "quenched reaction-zone mode" regime, neither OH nor temperature gradients are visible. Finally, in the "hot non-reacting holes" regime, temperature gradients are visible but no OH is detectable.

The current LES is being conducted for conditions that suggests that the flame type moves from the TRZ regime to the BRZ mode of burning as the equivalence ratio is decreased (see Fig. 1). Thus, flame stretch and local quenching effects should occur as Φ is decreased, and this effect should be reflected in CO, OH and reaction rate profiles. Here, flame structures obtained from Mechanisms B (cases 3 and 4) and C (cases 5 and 6) are analyzed in some detail. Since the trend toward local quenching within the sub-grid (when finite-rate, multi-step kinetics is employed in LEMLES) is of primary focus in this study, only the lower equivalence ratio cases are discussed in some depth. For brevity, only case 5 is discussed below, although the conclusions here are also valid for the corresponding case 3. Cases 4 and 6 are at higher Φ and shows even less sensitivity to local quenching effect and therefore, are not directly relevant for the current discussion.

A typical instantaneous flame structure and CO mass fraction contours are shown in Fig. 4. The flame structure is identified here as an iso-surface for $\widetilde{T} = 1500K$, where $\widetilde{T}$ is the LES-resolved temperature field. The CO concentration is also shown as a LES-resolved property that is obtained by ensemble averaging the sub-grid CO values from the LEM domains. The flame structure is highly compact and wrinkled due to the highly turbulent swirling flow entering the combustor.

The CO formation in the flame zone is further analyzed. The CO isolines in the flame region is shown in more detail in Fig. 5. It can be seen that the CO field is highly non-uniform in flame region with areas of high concentration and low concentration adjacent to each other. The magnitude of CO concentration depends also on the curvature and thickness of the flame and since the flow is unsteady, the curvature of the flame changes in time. Thus, CO mass fraction is dependent on the unsteady flame stretching and its spatial distribution changes with time. In the current study, flame stretch can occur in two manners: stretching due to large-scale eddies that are resolved on the LES grid and sub-grid straining by the stirring model used in the LEM. However, no explicit analysis of the stretch effect has been conducted so far.

A front view of the LES-filtered OH and T fields are shown in Figs. 6a and 6b, respectively for case 5. (Note that only Mechanism C has both NO and OH species). The flame exhibits regions where the amount of OH is quite low and wherever the amount of OH is low, the temperature field exhibits a thickening of the preheat zone. This is clearly shown in Figs. 7a and 7b which are close-up of the left middle part of the flame zone shown in Figs. 6a and 6b, respectively. The flame is locally highly curved in regions where OH mass fraction is low. Since the flow is unsteady (and highly swirling), the flame curvature is not constant. Therefore, it is logical to assume that regions with high flame curvature also corresponds to regions with high strain rates. Flame stretching (flame stretch being the sum of flame curvature and strain[39]) causes the reaction rate, and subsequently the OH mass fraction, to decrease. As the flame propagation speed decreases, the influence of turbulent convection becomes more important and leads to flame broadening, as observed in Fig. 7b.

To summarize, results suggest that high flame stretching leads to a decrease in the flame reaction rate and, as the reaction rate diminishes, turbulent mixing due to small and large scales tend to affect the flame by increasing the preheat region of the flame. However, temperature isolines are continuous and no total flame quenching is observed (Figs. 6b and 7b) for the conditions simulated here. The implication of this observation is discussed in the next section.

Figures 8a and 8b show, respectively, the isolines of OH concentration and the CH_4 reaction rate in a side view of the flame structure for case 5. The edge of

the inlet pipe expansion inside the combustion chamber is located in the upper left corner of the figures. Again, the OH mass fraction is highly non uniform along the flame front. The fuel reaction rate exhibits the same trend as the OH mass fraction. This agree with the fact that OH is directly linked with the rate of consumption of fuel.[40]

Analysis of the results show that the non-uniformities in the OH field occur when the flame is curved by large-scale structures. Furthermore, the flame broadens downstream of the inlet. A possible explanation is that as the thin flame front becomes stretched, the reaction rate (and the propagation speed) decreases. The chemical time scale decreases and becomes of the order of magnitude of the small eddy time scale. The small-scale eddies broaden the flame zone via turbulent convection. Finally, the broaden flame encounters the next coherent structure present in the shear layer and the process continues.

4.4 Resolution of Quench Effect

The results reported in the previous section suggests that although the reaction rate and OH concentration is reduced in regions of high stretch, the flame is not fully extinguished for cases 3-6 (note that, for cases 1 and 2, a model of flame extinction was used to force flame extinction). The emission predictions (Table 4) show UHC emission via flame quenching (as modeled by the ITNFS model). The 8-species and the 9-species mechanism can predict flame quenching.[25] In past LEM studies,[23] simulation of a flame propagation on a single LEM domain was successful in predicting flame propagation in the flamelet, thin-reaction zone and broken reaction zone (where local quenching was observed) regimes without requiring any model adjustments. Thus, it appears that the current LEMLES with Mechanism B or C is unable to account for flame extinction even though all elements of the approach when combined have the potential for achieving this goal. Clearly, some physics of the effect of flame stretch on extinction is missing in these simulations. Analysis discussed below provides a possible explanation and a mean to deal with this missing feature.

It has been noted in past studies that flame stretching is caused by eddies that can wrinkle the flame structure due to curvature, and strain the flame due to local turbulent straining. For a given case, this requirement may not be satisfied by all eddies. Meneveau's[5] study concluded that very small scale eddies are not powerful enough to induce noticeable flame stretch and to perturb the reaction processes. Therefore, there is a lower limit on eddies that can impact stretch and hence, the quenching process in a highly turbulent flow.

There are two mechanisms that account for the effect of turbulent eddies on flame stretch in LEMLES. In LEMLES, it is implicitly assumed that all eddies larger than $\overline{\Delta}$ are resolved on the 3D LES and therefore, all these eddies are expected to play their proper role in flame stretching. The other mechanism in LEMLES is the model for the effect of eddies smaller than $\overline{\Delta}$ on the scalar field implemented inside each LES grid. This model uses the sub-grid triplet mapping[41,42] to account for the increase in flame curvature (e.g., the distance between two flame crossings in the 1D LEM line is approximately twice the local radius of curvature[42]). It is apparent that both these mechanisms are missing something.

To determine this missing feature, it is instructive to review what LEMLES is actually resolving in space and time. For a typical case 5, Fig. 9a shows that the flame thickness is resolved at the LES level $\overline{\Delta}$ and that the reaction zone δ_{RR} is resolved at the LEM level. The effect of a typical sub-grid eddy ($\overline{\Delta}_{LEM-Eddy}$) (which is of the order of (δ_{RR}) is explicitly included in the stirring model in LEM. The various time scales are also reasonably well resolved, as shown in Fig. 9b. The reaction-diffusion equations evolve at the characteristic time step, which is a minimum of the diffusion time step, Δt_{diff} and the chemical time step Δt_{chem}. In the current study, $\Delta t_{diff} = \Delta t_{chem}$, and direct integration (using ISAT) is used to evolve the finite-rate kinetics. Δt_{stir} is the stirring time interval which decreases with increase in u', and as a result, a large number of stirring events occur in regions of high u' (e.g., shear layer).

The above analysis shows that the scalar field is well resolved by the LEMLES approach but that is not the case for all turbulent scales at the LES level. The typical LES grid resolution $\overline{\Delta}$ is 0.5 to 0.7 mm in the current study (note that, the LES resolution is required to be $coarse$, by definition). To resolve a typical eddy on the LES grid, approximately 4-5 grid points are needed from a numerical point of view. Thus, eddies of size 2.5 to 3.5 mm are properly resolved on the LES grid. Such eddies should therefore, properly wrinkle and/or stretch the flame (note that the flame is resolved at $\overline{\Delta}$ due to the LEM model).

At the sub-grid level, the $effect$ of small eddies (smaller than $\overline{\Delta}$) is modeled in the LEM model. Since we use 6 LEM cells to represent a sub-grid eddy,[41] the effect of eddies of 0.25 to 0.35 mm, are included in the LEM model.

It follows that eddies of sizes are between 2.5 mm and 0.5 mm are not resolved at both LES and LEM level in the current study. These length scales have to be compared with the flame thickness δ_f. For Φ=0.44, δ_f=0.681 mm. Therefore, eddies between δ_f - $4\delta_f$ are not resolved in this study. The implication of this observation is noted below.

The grid resolution, the LES resolution, the LEM resolution and the flame thickness are shown schematically in Fig. 10. Poinsot[4] established a criterion for

quenching limit as a function of the ratio of the eddy spinning velocity u' over δ_f and the ratio of the eddy size L over δ_f. u' is associated with the RMS value of the velocity field and is of the order of magnitude of 5 to 10 m/s in region of high shear (in the current study). For Φ=0.44, u' / δ_f is, therefore in the range of 50 to 100. For these values of u' / δ_f, the quenching limit is defined by values of L / δ_f between 3 and 5.

The above order of magnitude analysis shows that the length scale of eddies that are most likely to quench the flame front are not resolved at the LES level or at the LEM level. Eddies resolved at the LES level are large enough but their rotation speed may be too low when compared to the flame propagation speed. In this case, the flame surface is only wrinkled by these eddies and no quenching occurs. The eddies resolved at the LEM level are able to increase mixing in the flame region but are too small to quench the flame.

An obvious solution to this problem would be to increase the LES grid resolution by a factor of 4-5 in each direction (resulting in a 10-15 time increase in the grid resolution). However, such an increase would make such LES computationally impossible for all practical purposes. Just increasing the LEM resolution for the current LES grid size would also serve no purpose to capture quenching since very small eddies do not play an effective role in this process.

A possible solution (that is also computationally efficient) is to *increase* the domain of influence of the LEM model. That is, to extend the LEM domain to allow for eddy stirring on scales of the order of 4-5$\overline{\Delta}$ (note that the current LEM model restricts the subgrid domain to be less than $\overline{\Delta}$. In this case, the LEM domain will span over 4-5$\overline{\Delta}$ and eddies over a wider range will be allowed to stir the scalar fields. This approach will not compromise the resolution of the flame thickness δ_f, which will still be resolved at the LES grid level $\overline{\Delta}$. However, this approach may allow for larger eddies to perturb the scalar fields thereby, providing a mechanism to account for flame quenching. This extension of LEMLES is currently being considered.

5 Conclusion

Large Eddy Simulations (LES) of turbulent premixed combustion close to LBO in a gas turbine engine have been performed. A sub-grid combustion model based on the LEM model is implemented to simulate premixed combustion over a wide range of operational conditions, including combustion near LBO. Pollutant (CO and NO) formation is predicted using transport models using different chemical mechanism. For simple chemical mechanism, it is possible to predict emission of pollutants using a flamelet approach and by using a flame extinction model.

When no extinction model is employed but a more detailed chemical mechanism (which exhibits extinction in the laminar limit) is used in the LEMLES no extinction is observed even though decrease in both OH and fuel reaction rate is observed in regions of high stretch. Analysis of the results suggest that flame stretching and its effect on the flame propagation are captured, but that not all the relevant scales involved in flame extinction are properly resolved. In particular, it is shown that eddies smaller than 4-5$\overline{\Delta}$ but larger than $\overline{\Delta}$ are important scales that impact local flame quenching. However, in the current LEMLES, such eddies are not resolved properly and therefore, it fails to predict local quenching. A possible approach to deal with this problem within the LEMLES approach without requiring a drastic increase in LES resolution (and the associated cost) is suggested.

References

[1] Buschmann, A., Dinkelacker, F., Schaefer, T., Schaefer, M., and Wolfrum, J., "Measurement of the Instantaneous Detailed Flame Structure in Turbulent Premixed Combustion," *Twenty-Sixth Symposium (International) on Combustion*, 1996, pp. 437–445.

[2] Dinkelacker, F., Soika, A., Most, D., Hofmann, D., Leipertz, A., Polifke, W., and Doebbeling, K., "Structure of Locally Quenched Higly Turbulent Lean Premixed Flames," *Twenty-Seventh Symposium (International) on Combustion*, 1998, pp. 857–865.

[3] Najm, H. N., Paul, P. H., Mueller, C. J., and Wyckoff, P. S., "On the Adequacy of Certain Experimental Observables as Measurements of Flame Burning Rate," *Combustion and Flame*, Vol. 113, 1998, pp. 312–332.

[4] Poinsot, T., Veynante, D., and Candel, S., "Quenching processes and premixed turbulent combustion diagrams," *Journal of Fluid Mechanics*, Vol. 228, 1991, pp. 561–606.

[5] Meneveau, C. and Poinsot, T., "Stretching and Quenching of Flamelets in Premixed Turbulent Combustion," *Combustion and Flame*, Vol. 86, 1991, pp. 311–332.

[6] Held, T. J., Mueller, M. A., and Mongia, H. C., "A Data-Driven Model for NO_x, CO and UHC Emissions for a Dry Low Emissions Gas Turbine Combustor," *AIAA-2001-3425*, 2001.

[7] Eggenspieler, G. and Menon, S., "Modeling of Pollutant Formation near Lean Blow Out in Gas Turbine Engines," *Direct and Large Eddy Simulation V*, 2003.

[8] Kim, W.-W. and Menon, S., "LES of Turbulent Fuel/Air Mixing in a Swirling Combustor," *AIAA-99-0200*, 1999.

[9] Warhaft, Z., "Passive Scalars in Turbulent Flows," *Annual Review of Fluid Mechanics*, Vol. 32, 2000, pp. 203.

[10] Kerstein, A. R., "Linear-Eddy Model of Turbulent Transport II," *Combustion and Flame*, Vol. 75, 1989, pp. 397–413.

[11] Kim, W.-W., Menon, S., and Mongia, H. C., "Large-Eddy Simulation of a Gas Turbine Combustor Flow," *Combustion Science and Technology*, Vol. 143, 1999, pp. 25–62.

[12] Kim, W.-W. and Menon, S., "Numerical Simulations of Turbulent Premixed Flames in the Thin-Reaction-Zones Regime," *Combustion Science and Technology*, Vol. 160, 2000, pp. 119–150.

[13] Stone, C. and Menon, S., "Adaptive swirl control of combustion instability in gas turbine combustors," *Proceedings of the Combustion Institute*, Vol. 29, 2002, pp. 155–160.

[14] Sankaran, V., Porumbel, I., and Menon, S., "Large-Eddy Simulation of a Single-Cup Gas Turbine Combustor," *AIAA-2003-5083*, 2003.

[15] Erlebacher, G., Hussaini, M. Y., Speziale, C. G., and Zang, T. A., "Toward the Large-Eddy Simulation of Compressible Turbulent Flows," *Journal of Fluid Mechanics*, Vol. 238, 1992, pp. 155–185.

[16] Smagorinsky, J., "General Circulation Experiments with the Primitive Equations," *Monthly Weather Review*, Vol. 91, No. 3, 1993, pp. 99–164.

[17] Menon, S., Yeung, P.-K., and Kim, W.-W., "Effect of Subgrid Models on the Computed Interscale Energy Transfer in Isotropic Turbulence," *Computers and Fluids*, Vol. 25, No. 2, 1996, pp. 165–180.

[18] Kim, W.-W. and Menon, S., "A New Incompressible Solver for Large-Eddy Simulations," *International Journal of Numerical Fluid Mechanics*, Vol. 31, 1999, pp. 983–1017.

[19] Chakravarthy, V. and Menon, S., "Large-Eddy Simulations of Turbulent Premixed Flames in the Flamelet Regime," *Combustion Science and Technology*, Vol. 162, 2000, pp. 1–48.

[20] Chakravarthy, V. and Menon, S., "Subgrid Modeling of Premixed Flames in the Flamelet Regime," *Flow, Turbulance and Combustion*, 2001.

[21] Menon, S., McMurtry, P., and Kerstein, A. R., "A Linear Eddy Mixing Model for Large Eddy Simulation of Turbulent Combustion," *LES of Complex Engineering and Geophysical Flows*, edited by B. Galperin and S. Orszag, Cambridge University Press, 1993.

[22] Pope, S. B., "PDF Methods for Turbulent Reactive Flows," *Progress in Energy and Combustion Science*, 1985, pp. 119–192.

[23] Sankaran, V. and Menon, S., "The Structure of Premixed Flame in the Thin-Reaction-Zones Regime," *Proceedings of the Combustion Institute*, Vol. 28, 2000, pp. 203–210.

[24] Westbrook, C. K. and Dryer, F. L., "Simplified Reaction Mechanisms for the Oxidation of Hydrocarbon Fuels in Flames," *Combustion Science and Technology*, Vol. 27, 1981, pp. 31–43.

[25] Card, J. M., Chen, J. H., Day, M., and Mahalingam, S., "Direct Numerical Simulation of Turbulent Non-Premixed Methane-Air Flames Modeled with Reduced Kinetics," *Studying turbulence using Numerical Simulation Databases - V*, 1994, pp. 41–54.

[26] Mallampalli, H. P. and Fletcher, T. H., "Evaluation of CH4/NOx Global Mechanisms Used for Modeling Lean Premixed Turbulent Combustion of Natural Gas," *96F-098*, 1996, Fall Meeting of the Western States Section of the Combustion Institute University of Southern California, Los Angeles, CA October 28-29, 1996.

[27] Kee, J. R., Rupley, F. M., and Miller, J. A., "CHEMKIN-II A Fortran Chemical Kinetics Package for the Analysis of Gas Phase Chemical Kinetics," Tech. Rep. SAND89-8009B, Sandia National Laboratories, 1992.

[28] Held, T. J. and Mongia, H. C., "Emissions Modeling of Gas Turbine Combustors using a Partially-premixed Laminar Flamelet Model," *AIAA-98-3950*, 1998.

[29] Cannon, S. M., Zuo, B., and Smith, C. E., "LES Predictions of Combustor Emissions From a Practical Industrial Fuel Injector," *ASME-2003-GT-38200*, 2003.

[30] Li, S. C. and Williams, F. A., "Reaction Mechanism for Methane Ignition," *ASME-2000-GT-145*, 2000.

[31] Eggenspieler, G. and Menon, S., "Finite Rate Chemistry Modeling for Pollutant Emission Prediction near Lean Blow Out," *AIAA-2003-4941*, 2003.

[32] Hill, S. and Douglas Smoot, L., "Modeling of Nitrogen Oxides Formation and Destruction in Combustion Systems," *Progress in Energy and Combustion Science*, Vol. 26, 2000, pp. 417–458.

[33] Poinsot, T. and Lele, S., "Boundary Conditions for Direct Simulations of Compressible Viscous Flow," *Journal of Computational Physics*, Vol. 101, 1992, pp. 104–129.

[34] Pope, S., "Computationally Efficient implementation of combustion chemistry using in situ adaptive tabulation," *Combustion Theory Modelling*, Vol. 1, 1997, pp. 41–63.

[35] Bhargava, A., Kendrick, D. W., Colket, M. B., Sowa, W. A., Casleton, K. H., and Maloney, D. J., "Pressure Effects on NO_x and CO emission in industrial gas turbines," *Trans. of the ASME*, Vol. 2000-GT-8, 2000.

[36] Lilley, G., "Swirl Flows in Combustion: A Review," *AIAA Journal*, Vol. 15, No. 8, 1977, pp. 1063–1078.

[37] Lefebvre, A. H., *Gas Turbine Combustion*, Taylor and Francis, 2nd ed., 1999.

[38] Borghi, R., "On the Structure and Morphology of Turbulent Premixed Flames," *Recent Advances in Aerospace Sciences*, edited by C. Casci and C. Bruno, Plenum Press, 1985, pp. 117–138.

[39] Law, C. and Sung, C. J., "Structure, Aerodynamics, and geometry of premixed flames," *Progress in Energy and Combustion Science*, Vol. 26, 2000, pp. 459–505.

[40] Turns, S. R., *An Introduction to Combustion. Concept and Applications*, Mac Graw Hill, 1999.

[41] Kerstein, A. R., "Linear-Eddy Modeling of Turbulent Transport. Part 6. Microstructure of Diffusive Scalar Mixing Fields," *Journal of Fluid Mechanics*, Vol. 231, 1991, pp. 361–394.

[42] Menon, S. and Kerstein, A. R., "Stochastic Simulation of the Structure and Propagation Rate of Turbulent Premixed Flames," *Proceedings of the Combustion Institute*, Vol. 24, 1992, pp. 443–450.

[43] Bédat, B. and Cheng, R. K., "Experimental Study of Premixed Flames in Intense Isotropic Turbulence," *Combustion and Flame*, Vol. 100, 1995, pp. 486–494.

[44] Mansour, M., Peters, N., and Chen, Y., "Investigation of Scalar Mixing in the Thin Reaction Zones Regime using a simultaneous CH-LIF/Rayleigh Laser Technique," *Proceedings of the Combustion Instutute*, Vol. 27, 1998, pp. 767–773.

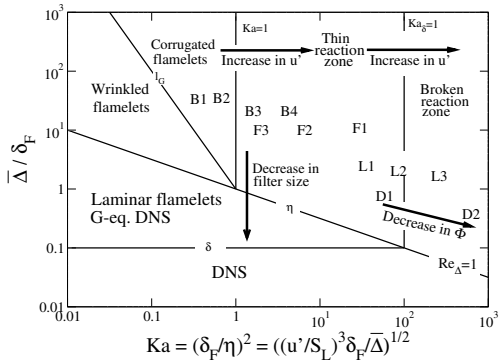

Fig. 1 Premixed combustion regimes and locations of typical flames: B-type,[43] F-type,[44] General Electric LM-6000[12] (L1: Φ=0.56, L2: Φ=0.53, L3: Φ=0.44) DOE-HAT combustor[7] (D1, for Φ>0.6 and D2, for Φ<0.5). Here, δ_F is the flame thickness, u' the sub-grid velocity fluctuations, S_L the laminar flame speed and $\overline{\Delta}$ is the grid size.

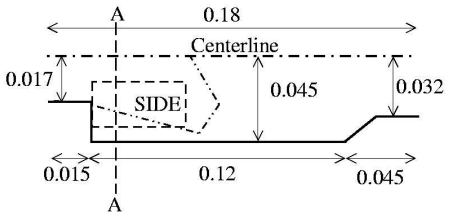

Fig. 2 Sketch of the combustion chamber geometry and dimensions. Dimensions are given in meters. – - - –: typical flame front location, – - –: combustion chamber centerline, AA: front view plane, SIDE: side view box.

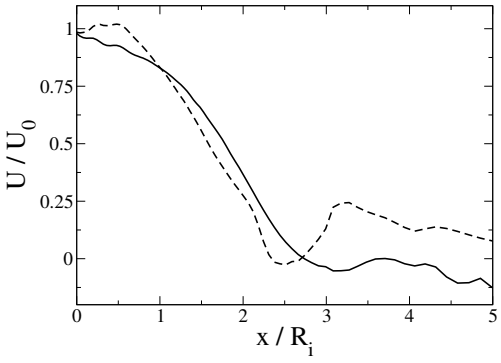

b) Mean velocity profiles at various axial locations

Fig. 3 Mean centerline axial velocity decay and mean velocity profiles at various axial locations. — : Φ=0.53 (case 4); - - : Φ=0.44 (case 3). R: combustion chamber radius, U_0: maximum inflow velocity (U_0=120$m.s^{-1}$), R_i: inflow pipe radius.

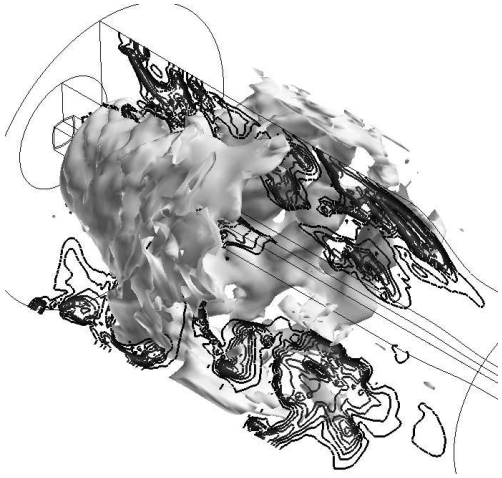

a) Case 3

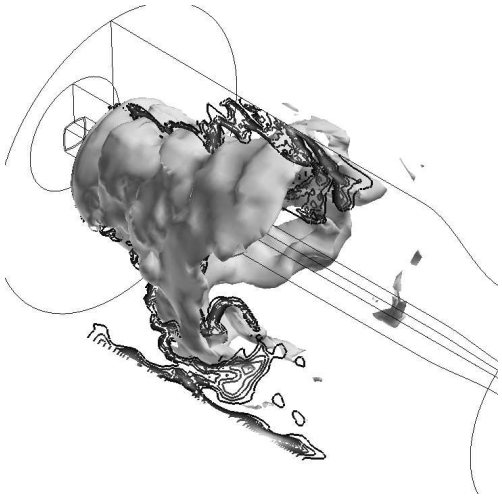

b) Case 4

Fig. 4 Flame isosurface ($\widetilde{T} = 1500.0$) and CO mass fraction isolines ($0 < \widetilde{Y_{CO}} < 500$ ppm).

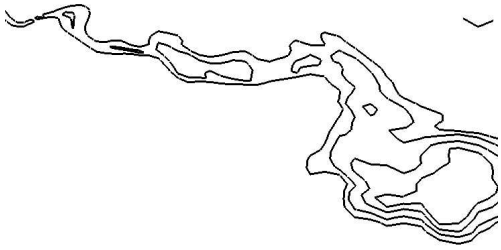

Fig. 5 Closeup of the flame zone CO contours interval. Side view. Case 5.

a) Isolines of OH concentration.

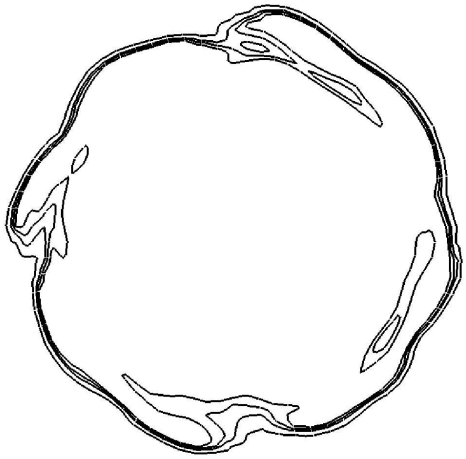

b) Isolines of temperature.

Fig. 6 Front View of the flame at x/R_i=0.75 for case 5.

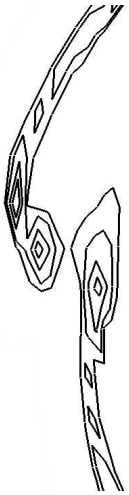

a) Isolines of OH concentration . Contours interval.

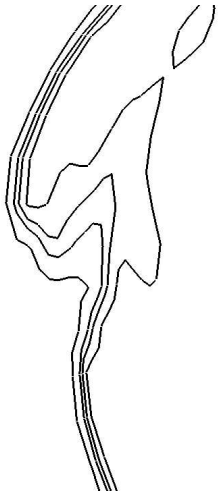

b) Isolines of temperature. Contours interval.

Fig. 7 Closeup of the flame region in the front view at x/R_i=0.75 for case 5.

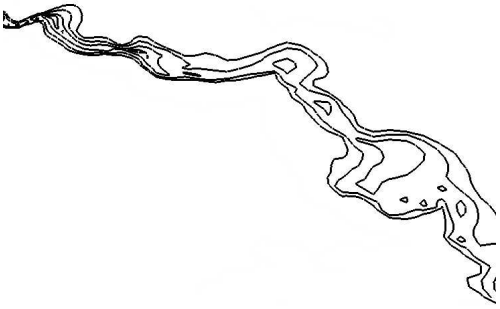

a) Isolines of OH concentration. Contours interval.

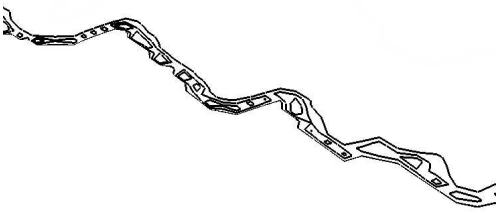

b) Isolines of CH_4 reaction rate. Contours interval.

Fig. 8 Closeup of the flame region in the side view for case 5.

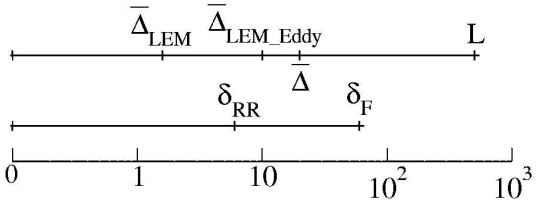

a) Length scales

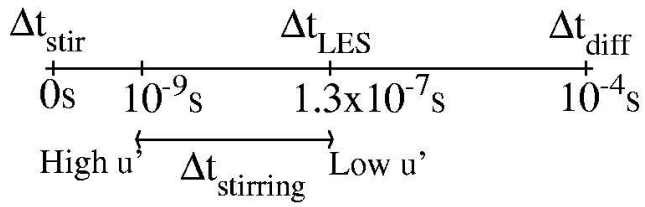

b) Times scales. Δt_{stir} is the triplet mapping time (instantaneous - $\Delta t_{stir} = 0$)

Fig. 9 Length and time scale resolution for Φ=0.44 in the LM 6000.

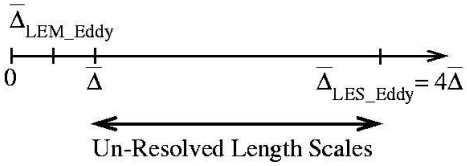

Fig. 10 Relative length of the smallest eddy resolved at the LEM level ($\overline{\Delta}_{LEM-Eddy}$), the smallest eddy resolved at the LES level ($\overline{\Delta}_{LES-Eddy}$) and the grid cell size ($\overline{\Delta}$). The flame thickness δ_F is equal to $\overline{\Delta}$.